liu hui (Orcid ID: 0000-0002-7959-0984)

Occurrence and Detection of Impact Multipath Simulations of Bending Angle

Quality Control of Bending Angle Simulations

Xiaolei Zou[1, *], Hui Liu[1, 2] and Ying-Hwa "Bill" Kuo[2]

[1]Cooperative Institute for Climate and Satellites, Earth System Science Interdisciplinary Center, University of Maryland, College Park, MD 20740 (***Contact:** *xzou1@umd.edu*; Phone: 301-405-1532)

[2]COSMIC, University Corporation for Atmospheric Research, Boulder, CO 80307

Abstract

In the moist tropical lower troposphere, atmospheric refractivity fields are strongly affected by water vapor and have complicated, non-spherically symmetric structures. Strong horizontal gradients of refractivity could make the simulated bending angle by raytracing a multivalued function of the impact parameter, which is called impact multipath for brevity. In this study, we first show such occurrences of impact multipath in the tropical lower troposphere using the National Centers for Environmental Prediction/Global Forecast System analysis as input to a raytracing operator for COSMIC ROs in March and April 2017. An up to 600-m lift in altitude for the impact parameter is observed for simulated RO rays in the presence of a strong horizontal gradient of refractivity over 250-km distances from the perigee, rendering the simulation bending angles multivalued functions of impact parameter. A quality control procedure is then developed to effectively identify the large variaitions of parameter along the simulated rays and impact multipath simulations while keeping the simulated rays below and above the multivalued rays. Many more RO data in the boundary layer could be used for data assimilation in numerical weather prediction by not removing the RO data below the impact multipath levels in the moist tropical lower troposphere.

Keywords: Detecting occurrence of multi-path simulation of bending angle

1. Introduction

The Constellation Observing System for Meteorology, Ionosphere, and Climate 2 (COSMIC-2) soon to be launched is optimized for data coverage over the tropics by having a three-times smaller inclination (24°) and a twice higher sampling rate (100 Hz) than those of COSMIC

(72° inclination and 50-Hz sampling rate). It will provide many more radio occultation (RO) retrievals in the tropical lower troposphere than ever before. The RO variable assimilated into numerical weather prediction (NWP) data assimilation systems is the bending angle as a function of the impact parameter (Zou et al., 1999, 2000; Palmer et al., 2000; Liu and Zou, 2003; Zou et al., 2004; Poli and Joiner, 2004; Healy et al., 2007). The bending angle is derived from time series of excess Doppler shift measurements and by assuming spherical symmetry, i.e., that the atmospheric refractivity field is a function of the radial distance only (Melbourne et al., 1994; Jensen et al., 2003; Gorbunov et al., 2004). As a result, the impact parameter is assumed to remain constant along a ray path. But atmospheric refractivity in the tropical lower troposphere is strongly affected by water vapor. The refractivity field is thus not spherically symmetric and has strong horizontal gradients, making the impact parameter vary along a ray path (Gorbunov et al., 1996; Healy, 2001). Since RO retrievals of bending angle are the total bending of the rays going from GPS to LEO satellites, an accurate non-local observation operator is required for generating model simulations in an atmosphere whose refractivity is not spherically symmetric. This is especially the case for COSMIC-2 related applications involving model simulations such as RO data assimilation and real-time monitoring.

Applications of non-local observation operators of bending angle to RO data assimilation have been successful. Zou et al. (1999) and Liu et al. (2001) developed a 2D raytracing operator of bending angle and demonstrated the positive impact of assimilating a small number of bending angle profiles (837 RO profiles from GPS/Meteorology) over an 11-day period i.e. 20-30 June 1995 on the 5-day forecast. Healy (2014) implemented a 2D bending

angle operator into the European Centre for Medium-Range Weather Forecasts (ECMWF) assimilation system and demonstrated a better fit of the ECMWF analysis to RO bending angle retrievals and a positive impact on global forecasts.

In the tropical lower troposphere where NWP background fields have extremely large horizontal gradients, e.g., associated with small-scale water vapor and convective clouds, the impact parameter can vary significantly along a ray path (several hundreds of meters). The simulated bending angle by the raytracing method could then become multivalued functions of the impact parameter at the end of the simulated ray (S. Sokolovskiy, personal communication). On the other hand, RO bending angle retrievals are derived by wave-optics including full spectrum inversion and phase matching under the assumption of spherical symmetry (Gorbunov, 2002b; Jensen et al., 2003, 2004; Gorbunov and Lauritsen 2004). Therefore, the so-called multipath, which is usually associated with multiple rays arriving at a receiver at a given time, is mitigated by RO data processing techniques, and GPS RO bending angle profiles retrievals are single-valued functions of the impact parameter. The RO bending angle retrievals have larger uncertainty in the presence of stronger horizontal gradients. One measure of the uncertainty can be provided by the local spectra width of the bending angle noise in the wave-optics approach (Liu et al., 2018). Liu et al. (2018) showed that not using bending angle retrievals being characterized by large local spectral width improved the forecast performance in a relatively basic NWP model. This study aims at identifying the cases of large variations in the impact parameter along simulated rays and the multivalued raytracing simulations and developing a quality control procedure to remove these data from RO data assimilation.

The paper is organized as follows. Section 2 describes a 2D raytracing operator and the input data to the raytracing operator for generating one and a half months of model simulations. Section 3 illustrates the variations in the impact parameter along a ray path in the presence of a strong horizontal gradient of refractivity causing a multivalued bending angle profile simulation. A quality control procedure for identifying the occurrences of impact multipath in model simulations due to strong horizontal gradients of refractivity is developed and its impact on the differences in bending angle between model simulations and RO retrievals are assessed in section 4. Section 5 summarizes the findings and conclusions.

2. A brief description of a raytracing operator and input data for generating simulations

The 2D raytracing operator used in this study solves the following second-order ordinary differential equation (Zou et al., 1999; Liu and Zou, 2003):

$$\frac{d^2\vec{r}}{d\tau^2} = n\nabla n, \qquad (1)$$

…where $\vec{r}$ is the 3D position vector in Cartesian coordinates [$\vec{r}$ = (x_1, x_2, x_3)], and τ is a parameter associated with the length of the ray (s) and the atmospheric index of refractivity (n), i.e. $d\tau = \frac{ds}{n}$.

The second-order ray trajectory Equation 1 can be equivalently turned into the following two coupled first-order equations:

$$\begin{cases} \frac{d\vec{r}}{d\tau} = \vec{y} \\ \frac{d\vec{y}}{d\tau} = n\nabla n \end{cases}. \qquad (2)$$

To solve Equation 2, an initial condition of ($\vec{r}$, $\vec{y}$) at the starting position (in this study, the observed ray perigee) is required.

Denote the position of a point on the ray by a radius vector from the local center of curvature to the point ($\vec{r}$), the radius vectors at the GPS and LEO positions by $\vec{r}_G$ and $\vec{r}_L$, respectively, and the perigee point of the ray that has the shortest distance ($\vec{r}_0$) from the ray to the earth's local curvature center. The impact parameter (a) at a point on the ray is defined as the distance from this point on the ray to the earth's local curvature center multiplied by the index of refractivity, i.e.

$$a = rn(r)\sin\phi, \tag{3}$$

…where ϕ is the angle between the tangent direction of the ray and the local radius vector. The impact parameter at the perigee ($\phi = 90°$) is thus $a_0 = r_0 n(r_0)$. If the atmosphere is spherically symmetric, the impact parameter satisfies Bouguer's formula:

$$a = rn(r)\sin\phi = const \tag{4}$$

The spherical symmetry also ensures that the ray path remains in the "occultation plane", i.e. the plane that contains the LEO and GPS satellite positions and the origin of the coordinate system.

A ray integration of Equation 2 starts from the estimated perigees of COSMIC ROs at a vertical interval of 100 m in the direction of the observed ray propagation. This perigee and azimuth information is provided by COSMIC along with retrievals of bending angle profiles as functions of impact parameter and ends at the 20,200-km and 730-km distances above the earth's surface for the modeled GPS and LEO satellite positions, respectively. The ray integration uses a variable step size of 2 km or smaller. Values of the impact parameter along

the ray path are calculated as the ray integration continues. The bending angle at the impact height $[\alpha(a)]$ is finally computed as the angle between the tangent vector at the GPS satellite ($\vec{t}_G$) and the tangent vector at the LEO satellite $\vec{t}_L$ of the ray, i.e.

$$\alpha = \angle(\vec{t}_G, \vec{t}_L). \quad (5)$$

This study uses National Centers for Environmental Prediction (NCEP) global forecast system (GFS) analyses and COSMIC observations from 19 March to 30 April 2017 in the latitudinal band 30°S to 30°N. Model simulations are performed for 6,040 bending angle profiles.

A special version of NCEP GFS analyses is used as the model atmosphere for bending angle simulations. The horizontal resolution is 0.25° × 0.25° and there are 31 vertical pressure levels from the surface to ~1 hPa (~48 km). The vertical resolutions are 25 hPa below the 900-hPa level and 50 hPa between 900 and 100 hPa. The refractivity above the top height of the GFS analysis is calculated using the Committee on Space Research International Reference Atmosphere (CIRA) model. The CIRA model is a middle-atmosphere model presented as tabulations of atmospheric properties (temperature, pressure, and zonal wind) as functions of latitude, height, and time of year (Rees et al., 1990). The index of atmospheric refractivity is assumed to be unity above 120 km. Earth is assumed to be spherical with the local curvature radii from the COSMIC ROs. The refractivity is first calculated from temperature, pressure, and specific humidity at the GFS and CIRA model grid points. This is then interpolated to the ray position using spline and linear interpolations in the vertical and horizontal directions, respectively.

3. Identification of occurrences of impact multipath simulations

3.1. Along-track variations of impact parameter and bending angle

The non-negligible horizontal gradient of refractivity makes the spherical symmetry assumption invalid and Equation 4 no longer exact. In other words, the impact parameter (a) is not constant over the ray path. The rate of change of the impact parameter along the ray path can be calculated by the following formula (Gorbunov et al., 1996):

$$\frac{da}{ds} = \left(\frac{\partial n}{\partial \theta}\right)_r, \qquad (6)$$

…where θ is the angle defined by $\theta = \angle(\vec{r}_G, \vec{r})$ and $(\partial n/\partial\theta)_r$ is the partial derivative of refractive index with respect to θ at the point $\vec{r}$ on the ray. The latter is called the along-track horizontal gradient of the refractive index. Since our raytracing simulations start at the perigee (Zou et al., 1999; Liu and Zou, 2003), the variation of the impact parameter at any point ($\vec{r}$) on the integrated ray path can be written as

$$(\Delta a)_{s_i} = a_{s_i} - a_0 = \int_{r_o}^{s_i} \left(\frac{\partial n}{\partial \theta}\right)_r ds, \qquad (7)$$

…where s_i represents the grid points for the integration of Equation 2. The differences in impact parameter values at the GPS and LEO satellite positions s_G and s_L from the perigee are denoted by $(\Delta a)_{s_G}$ and $(\Delta a)_{s_L}$, respectively. The spherical asymmetry assumption becomes invalid if $(\Delta a)_{s_i}$ ` 0 for a given ray path.

In the 2D occultation plane, the dependence of the along-track change in bending angle on the gradients of refractive index within the occultation plane can be expressed in polar coordinates [$(\vec{r}, \theta)$; Eyre, 1994; Healy, 2001]:

$$\delta\alpha = -\frac{1}{n}\left(\frac{\partial n}{\partial r}\right)_\theta r\delta\theta + \frac{1}{n}\left(\frac{\partial n}{\partial \theta}\right)_\theta \frac{\delta r}{r}. \qquad (8)$$

At the perigees where most of the bending occurs, the contribution of the along-track gradient of the refractive index to the total bending angle is zero by definition because $\left(\delta r/r\right)_{\vec{r}_0} = \delta\theta \cot\angle\left(\vec{t}_0, r_0\right) = 0$. It is the vertical gradient of refractive index $[(\partial n/\partial r)_\theta]$ that contributes mostly to the total bending angle.

3.2. A detailed analysis of individual occultation events

Here, how simulations of bending angle are found to be multivalued or equivalently have impact multipath is explained. For a setting RO, the impact parameter representing the altitudes of rays decreases as the rays go down toward the earth's surface under the spherical symmetry condition. When a strong horizontal gradient of refractivity exists, the impact parameter varies along some ray paths so that its values at the LEO and/or GPS satellite positions (i.e., the two ends of the ray integration started at the perigee point) may be larger than those rays whose perigee points are higher. Occurrences of multivalued bending angle simulations depend on the specified vertical interval of the simulated rays at the perigee. Denser intervals of rays would allow identification of more multivalued bending angle simulations affected by weak and small-vertical-extent horizontal gradients of refractivity. We choose the 100-m vertical interval for simulated rays at the perigee points in this study. Note that most operational assimilation systems assimilate RO bending angles at a coarse vertical resolution (e.g., a 200-m interval). Multivalued bending angle simulations may then show up only in cases of stronger horizontal gradients of refractivity of larger vertical extent. A COSMIC RO profile located at (37.9°W, 25.1°S) on 1450 UTC 19 March 2017 (RO1) is selected to show impact multipath occurrences in model simulations (Fig. 1). The simulated

impact parameter at the LEO satellite position decreases monotonically as the rays go from 5 km down to 3.69 km towards the earth's surface but increases as the rays' perigee altitudes decrease for the next two rays below the ray whose perigee altitude is at 3.69 km (Fig. 1a). The second ray below the ray at 3.69 km has an impact parameter of 3.86 km at the LEO satellite position, which is 0.35 km higher than the impact parameter at the perigee point (3.51 km). In fact, all rays whose perigee point altitudes are below (above) the 3.69-km altitude have larger (smaller) impact parameters at the LEO positions than at their perigee points, indicating that the simulated ray paths bend up (down).

The RO bending angle retrieval profile is a single-valued function of the impact parameter (Fig. 1b). However, the simulated bending angle profile is multi-valued when the impact parameter experiences large variations along the ray paths (~300-400 m, Fig. 1c) for those 4-5 rays whose perigee point altitudes are between 3.69 and 3.86 km, for which the simulated bending angles (~0.06 rad) are about 3-4 times larger than the retrievals (<0.03 rad; Fig. 1b). The NCEP GFS analysis inputted into the raytracing operator shows that a strong inversion layer was present at the altitude of the multivalued bending angle simulations (Fig. 1d). The vertical gradient of the refractivity at the perigee reaches a maximum value of -120 N-units km^{-1}. Results in Figs. 1 and 2 are of similar looking to those from radio-holographic analyses of some wave optics forward simulations by Gorbunov (2002a) and Gorbunov et al. (2010) (see Fig. 4 in Gorbunov et al., 2010).

Another example is the COSMIC RO event that was located at (3.0°W, 36.3°S) on 0245 UTC 19 March 2017 (RO2; Fig. 2). The largest difference in impact parameter between the perigee and the LEO satellite is about 150 m, which is much smaller than those for RO1. Simulations

of the bending angle for this RO event are multivalued in a much thinner vertical layer than for RO1 (Fig. 2b). The vertical gradients of refractivity for RO1 (Fig. 1d) and RO2 (Fig. 2d) have similar magnitudes.

The impact parameters at the LEO satellite positions for rays whose perigees are below 3 km (the lowest-altitude eight rays) have a systematic upward shift (~0.3 km) than at their perigees compared with the RO bending angles (Fig. 1b), although the vertical gradients of the GFS refractivity for these rays at the perigee are small (~40 N-units km^{-1}) and invariant with height (Fig. 1d). The systematic upward shift of the simulated impact parameter from the perigee to the LEO satellite position is less significant for the RO2 case which has a shallower layer of multivalued bending angles (Fig. 2b). To summarize, although not having a multivalued problem, the RO1 and RO2 simulations below the multivalued layers are still under the influence of the horizontal gradient of refractivity, causing the impact parameter to vary along the ray paths. This may be true in the real atmosphere when RO bending angle retrievals are affected by the horizontal gradients of refractivity in the lower tropical troposphere. The systematic upward shift of the simulated impact parameter at the LEO position from the perigee point could be real.

To see how the impact parameter varies along the ray paths, Figure 3 shows deviations of the impact parameter at any point along all simulated ray paths below 5 km from their values at the perigees for both RO1 and RO2 profiles. The impact parameter increases rapidly ~250-300 km from the perigee for rays with a_0 below 3.6 km and 3.3 km for RO1 and RO2, respectively. For RO1 (Fig. 3a), the impact parameter varies and remains constant when the rays' horizontal distances from the perigee are smaller and greater than 300 km, respectively.

It is reminded that when the horizontal distances of the rays from the perigee are greater than 300 km, their vertical altitudes are more than ~4 km higher than their perigee points (figure omitted). The variations in the impact parameter along the ray paths for RO2 (Fig. 3b) are similar to those of RO1 when it comes to propagation from the perigee to the LEO satellite position. The impact parameter for RO2 does not vary greatly below 5 km when the rays propagate from the GPS satellite to the perigee (Fig. 3b).

In what weather systems did the RO1 and RO2 events occur? The RO1 event was located at the tip of a trough located at the geopotential height of 850 hPa which roughly corresponds to the 3.5-km impact height (Fig. 4a). A narrow belt of maximum refractivity, a few hundreds of meters width with refractivity values above 300 N-units, is seen along the trough, oriented from southeast to northwest. The RO1 ray path cut through this belt nearly perpendicularly, with a maximum refractivity a few hundreds of meters from the RO's perigee on the LEO satellite side. The cross-section of refractivity and its dry and water vapor components along the observed ray propagation direction (Fig. 4b) indicates that a strong vertical gradient of GFS refractivity co-existed geographically with the streak of maximum horizontal gradient seen in Fig. 4a. A vertical lifting of large refractivity (i.e., a steep tilting of refractivity to the north) is found near the perigees on the LEO satellite side, resulting in large vertical gradients of refractivity (denser curves of refractivity) near the perigees. If we separate the dry and water vapor contributions to the total refractivity, the strong horizontal gradient of refractivity north of the perigee comes mainly from the water vapor contribution (solid curve in Fig. 4b) to the refractivity (shaded in colors in Fig. 4b).

The RO2 event was located on a ridge at ~36.3°S (Fig. 5). The rays went from southeast to northwest. A trough was located to the west of the ridge, characterized by a curving band of large refractivity values. Air with higher refractivity values intruded into the area north of the RO2's perigee location in a low refractivity region, creating a large along-track gradient of refractivity. The refractivity remained low south of the perigee location. This is consistent with the changes in impact parameter along the ray paths shown in Fig. 3b. Results concerning the vertical cross-section of refractivity and its dry and water vapor components along the ray propagation direction for RO2 (Fig. 5b) are similar to but with weaker increases in refractivity near the perigees on the LEO satellite side than those for RO1 (Fig. 4b).

The 3D variations in atmospheric refractivity lead to variations in the vertical gradients of the refractivity $[(\partial N/\partial r)_\theta]$ along the ray paths [see Equation 8] of the RO1 and RO2 events (Fig. 6). Near the perigees where most of the bending occurs, the large variations in along-track vertical gradients of refractivity are found between the layers where the differences in bending angle between RO retrievals and simulations are large (Figs. 1b and 2b). Large variations in along-track vertical gradients of refractivity are also found between the 100-250 km horizontal distances from the perigees, contributing to the differences in bending angle between retrievals and simulations seen at low levels in Figs. 1b and 2b. Figures 4-6 confirm that strong horizontal gradients often collocated with increased vertical gradients of refractivity to break the spherical symmetry assumption and to induce the impact multipath simulations.

3.3. Statistical results

A statistical analysis of the impact parameter variations along ray paths and bending angle simulations was done to assess how representative the results shown in section 3.b are. The COSMIC CDAAC team provided a total of 6,040 RO profiles in the latitudes from 60°S to 60°N from 19 March to 30 April 2018. Bending angle simulations were generated from these profiles. One thousand eighty of the RO profiles have multivalued bending angle simulations (Fig. 7a). Most of them are located in the subtropical oceanic area between 30°S and 30°N. Their impact heights are found between 2.8 and 3.6 km where strong inversions associated with the top of a stable marine boundary layer often occur (Sokolovskiy, 2003; Ao, 2007 etc). At higher latitudes (30°-60°S and 30°-60°N), many fewer multivalued simulations are found. The remaining 4,960 RO profiles whose bending angle simulations are single-valued are distributed everywhere (Fig. 7b).

Figure 8 shows profiles of the differences in impact parameter between the perigee and both the LEO and the GPS satellite positions in terms of the impact height at the LEO and GPS satellite positions. The multivalued bending angle simulations (Fig. 8a) have a much larger spread between 2.8 and 4 km than do the single-valued bending angle simulations (Fig. 8b). The largest positive values can reach 400–600 m around the 3.5-km impact height. The negative values are smaller in magnitude (~200 m). These differences in individual profiles are larger than the 100-m vertical interval for the ray paths at the starting point (perigee) of the ray integrations. The mean $(\Delta a)_{s_L}$ (green curve in Fig. 8a) has a small positive bias (~25 m) below 3.2 km because the abnormally large impact parameter differences causing multivalued bending angle simulations occur at different impact heights and the positive and negative differences cancel out. The differences in impact parameter between the perigee and

either the LEO or the GPS satellite positions without the multivalued problem have no bias and much smaller standard deviations (Fig. 8b) than the profiles with the multivalued problem (Fig. 8a).

Figures 9 and 10 statistically confirm the lack of impact multipath in COSMIC bending angle retrievals, the large deviations of model simulations from the retrievals, and the large vertical gradients of refractivity when simulations have impact multipath. The spaghetti maps of the vertical distributions of all RO profiles with multivalued bending angle simulations at some impact heights (cyan profiles in Fig. 9a) are significantly different from RO retrievals (Fig. 9b) below 4 km. The simulated bending angles for many profiles increase sharply in the impact height range of 2.8–3.5 km, reaching extremely large values of 0.04–0.08 rad (Fig. 9a). The corresponding bending angle retrievals vary smoothly with respect to the impact height and have a small spread (< 0.04 rad, Fig. 9b). Such differences between simulations and RO retrievals in the bending angle samples are systematic and are thus also seen in the mean profiles (green curves) between Figs. 9a and b.

In fact, the presence of impact multipath also has impact on 1D simulations. The spaghetti map of the vertical profiles of bending angle from 1D simulations (Fig. 10a) is more similar to the 2D simulations (Fig. 9a) than to RO retrievals (Fig. 9b). The 1D simulated bending angles also profiles that increase sharply in the impact height range of 2.8–3.5 km, much less smooth than RO bending angle retrieval profiles (Fig. 9b). It is also confirmed that multi- and large-valued bending angle simulations are associated with extremely large vertical gradients of refractivity (Fig. 10b).

4. A quality control (QC) procedure for detecting impact multipath simulations

About 18% of the bending angle simulations by the 2D raytracing operator from the NCEP GFS analysis are multivalued at the ends of the ray paths. QC of the simulations is needed to detect these data points so that they can be removed from the RO bending angle assimilation. The first QC step (QC1) eliminates the simulations affected by strong along-track horizontal gradients. The second QC step (QC2) further eliminates the simulations with differences in the impact parameter between the perigee and either the LEO or the GPS satellites [$(\Delta a)_{s_L}$ or $(\Delta a)_{s_G}$] greater than 200 m. This value is chosen because $(\Delta a)_{s_L}$ is generally less than 200 m for all single-valued ROs (see Fig. 8b), and 200 m is two times the vertical interval of the simulations. The third QC step (QC3) further eliminates all simulations below the multivalued layer. Figure 11 illustrates the implementation of these three QC steps for the same two RO profiles discussed in section 3.2. For RO1, the QC1 step removed four rays whose simulated bending angles are multi-valued, and the QC2 step removed all rays having impact heights lower than those removed by the QC1 step since $(\Delta a)_{s_L}$ is greater than 200 m (Fig. 11a). For RO2 (Fig. 11b), the QC1 step removed only one ray whose impact height at the perigee is 3.2 km. Data points removed by the QC3 step are seen below the height level of the data point removed by the QC1 step.

The overall effect of the QC1, QC2, and QC3 steps on simulated RO profiles can be seen from spaghetti maps of the differences in impact parameter, $(\Delta a)_{s_L}$ and $(\Delta a)_{s_G}$, in terms of the impact height at either the LEO or the GPS satellite positions (Fig. 12). Compared with Fig. 8a without any QC, the QC1 step effectively removed those large and upward tilting parts of the multivalued simulations (Fig. 12a). There are still several data points that have

differences greater than 200 m, which are all removed by the QC2 step (Fig. 12b). Figures 12a and 12b show positive $(\Delta a)_{s_L}$ or $(\Delta a)_{s_G}$ biases. The positive bias in Fig. 12b is slightly smaller than that in Fig. 12a. By removing all data points below the impact multipath rays, the $(\Delta a)_{s_L}$ or $(\Delta a)_{s_G}$ bias reduces to almost zero (Fig. 12c), and the standard deviations are comparable in magnitude with those from profiles without multivalued problems (Fig. 8b). Figure 13 shows the total data counts removed by the QC1, QC2, and QC3 steps. The data removed by the QC1 step represent rays with impact heights between 2.3 and 3.8 km. The maximum percentage of data points removed by the QC1 step is ~28% around the 3-km impact height (Fig. 13) and is confined in the 3.8-2.3-km layer. The QC2 step removes an additional percentage of data points (< 9%) within a similar range of impact heights as those removed by the QC1 step. As expected, a significant amount of data is removed by the QC3 step, e.g., more than half of the rays with impact heights below 3.2 km. The three QC steps are implemented sequentially. Depending on the application, users may choose to implement the QC1 step only if the sole concern is an impact multipath problem with the simulations. Based on the fact that there is residual bias after the QC1 and QC2 (Fig. 12b), including the QC3 step may be a conservative but safer choice.

The vertical variations in the means and standard deviations of the fractional differences in the bending angle simulations generated by the 1D local and 2D raytracing simulations (Fig. 14) are significantly larger if impact multipath profiles are included (red dashed curves) below the impact height of about 3.8 km. The 1D simulations have a positive bias around 5-10% below the 3-km impact height, which reduces to nearly zero after removing those ROs with impact multipath simulations detected by the proposed quality control procedure. In

other words, the quality control procedure identifying ROs with impact multipath simulations is also valuable to RO data assimilation using the 1D observation operator. The 2D forward operator will be required for the QC when assimilating with the 1D operator. Although both the means and standard deviations of the differences between RO retrievals and model simulations (1D or 2D) are reduced after eliminating the impact multipath profiles, both the 1D and 2D simulations still have large positive biases (~16% below the 3-km impact height).

5. Summary and conclusions

Bending angle simulations were generated from a 2D global raytracing operator with the NCEP/GFS high-resolution analysis as input for all COSMIC ROs in the tropical lower troposphere within (60°S, 60°N) from 19 March to 30 April 2017. Many (~18%) of the bending angle simulations at the ends of ray path integrations are found to be multivalued in terms of the impact parameter at either the GPS or the LEO satellite positions. Most of these multivalued simulations are located in the low latitudes (30°S-30°N) around the 3.2-km impact height, resulting from strong along-track gradients of refractivity causing large variations (~100-600 m) in the impact parameter along the simulated ray paths. A three-step quality control procedure was developed for identifying multivalued simulations as well as those below and above the multivalued layers for which the spherical symmetry assumption fails. Simulations from both the 1D and 2D operators have much improved accuracy after applying the quality control.

The results obtained in this study may be specific to the raytracing operator and the NCEP GFS analysis. The gradient of refractivity in the tropical lower troposphere of other NWP

models at higher resolutions may be stronger. Future work will assess and report on the impacts of incorporating the three quality control steps on RO data assimilation and NWP forecasts in the tropical troposphere.

Acknowledgements

The second author thanks Dr. Sergey Sokolovskiy for helpful discussions related to this study. This research was jointly supported by National Oceanic and Atmospheric Administration Grant NA14NES4320003 and the collaborative project between the University Corporation for Atmospheric Research and the Taiwan National Space Program Office.

References

Ao, CO. (2007) Effect of ducting on radio occultation measurements: An assessment based on high-resolution radiosonde soundings. *Radio Sci.*, **42**, RS2008, https://doi.org/10.1029/2006RS003485.

Eyre, J. R. (1994) Assimilation of radio occultation measurements into a numerical weather prediction system. ECMWF Tech. Memo. **199**, 35 pp., https://www.ecmwf.int/sites/default/files/elibrary/1994/9331-assimilation-radio-occultation-measurements-numerical-weather-predictionsystem.pdf.

Gorbunov, ME, Sokolovsky S.V., and Bengtsson L. (1996) Space refractive tomography of the atmosphere: modeling of direct and inverse problems. Max-Planck Inst. fur Meteorol. Rep. 210, 59 pp.

Gorbunov, M. E. (2002a) Radio‐holographic analysis of Microlab‐1 radio occultation data in the lower troposphere, *J. Geophys. Res*., **107** (D12), 4156, doi:10.1029/2001JD000889.

Gorbunov, M. E. (2002b) Canonical transform method for processing radio occultation data in the lower troposphere. *Radio Sci.*, **37**(5), 1076, https://doi.org/10.1029/2000RS002592.

Gorbunov, M. E., and Lauritsen K. B. (2004) Analysis of wave fields by Fourier integral operators and its application for radio occultations. *Radio Sci.*, **39**, https://doi.org/10.1029/2003RS002971.

Gorbunov, M. E., Lauritsen K. B., and Leroy S. S. (2010) Application of Wigner distribution function for analysis of radio occultations. *Radio Sci.*, **45**, RS6011, doi:10.1029/2010RS004388.

Healy, S. B. (2001) Radio occultation bending angle and impact parameter errors caused by horizontal refractive index gradients in the troposphere: A simulation study. *J. Geophys. Res. Atmos.*, **106**, 11,875–11,889, https://doi.org/10.1029/2001JD900050.

Healy, S.B. (2014) Implementation of the ROPP two-dimensional bending angle observation operator in an NWP system. ROM SAF Report 19, 33 pp, http://www.romsaf.org/general-documents/rsr/rsr_19.pdf.

Healy S.B., Eyre J.R., Hamrud M., and Thépaut J.-N. (2007) Assimilating GPS radio occultation measurements with two-dimensional bending angle observation operators. *Q. J. R. Meteorol. Soc.*, **133**, 1213–1227, https://doi.org/10.1002/qj.63.

Jensen, A. S., Lohmann M. S., Benzon H., and Nielsen A. S. (2003) Full spectrum inversion of radio occultation signals. *Radio Sci.*, **38** (3), 1040, https://doi.org/10.1029/2003RS002763.

Jensen, A. S., Lohmann M. S., Nielsen A. S., and Benzon H. (2004) Geometric optics phase matching of radio occultation signals. *Radio Sci.*, **39**, RS3009, https://doi.org/10.1029/2003RS002899.

Liu, H., and Zou X. (2003) Improvements to a GPS radio occultation raytracing model and their impacts on assimilation of bending angle. *J. Geophys. Res. Atmos.*, **108**, D17, 4548, https://doi.org/10.1029/2002JD003160.

Liu, H., Zou X., Shao H., Anthes R., Chang J., Tseng J., and Wang B. (2001) Impact of 837 GPS/MET bending angle profiles on assimilation and forecasts for the period June

20–30, 1995. *J. Geophys. Res*. *Atmos.*, **106**(D23), 31,771–31,786, https://doi.org/10.1029/2001JD000345.

Liu, H., Kuo Y.-H., Sokolovskiy S., Zou X, Zeng Z., Hsiao L.-F., and Ruston B. (2018) A quality control procedure based on bending angle measurement uncertainty for radio occultation data assimilation in the tropical lower troposphere. *J. Atmos. Ocean. Tech.*, (in press), https://doi.org/10.1175/JTECH-D-17-0224.1.

Melbourne, W.G., Davis E.S., Duncan C.B., Hajj G.A., Hardy K. R., Kursinski E.R., Meehan T.K., Young L.E., and Yunck T.P. (1994) The application of GPS to atmospheric limb sounding and global change monitoring. JPL Pub. 94-18, 159 pp., https://ntrs.nasa.gov/archive/nasa/casi.ntrs.nasa.gov/19960008694.pdf.

Poli, P., and Joiner J. (2004) Effects of horizontal gradients on GPS radio occultation observation operators. I: Raytracing. *Q. J. Roy. Meteor. Soc.*, **130**, 2787–2805, https://doi.org/10.1256/qj.03.228.

Rees, D., Barnett J.J., and Labitzke K. (1990) COSPAR International Reference Atmosphere. II: Middle atmosphere models. *Adv. Space Res*., **10**(12), 517 pp.

Sokolovskiy S. (2003) Effect of super-refraction on inversions of radio occultation signals in the lower troposphere. *Radio Sci.*, **38**(3), 1058, https://doi.org/10.1029/2002RS002728.

Zou, X., Vandenberghe F., Wang B., Gorbunov M.E., Kuo Y.H., Sokolovskiy S., Chang J.C., Sela J.G., and Anthes R.A. (1999) A raytracing operator and its adjoint for the use of GPS/MET refraction angle measurements. *J. Geophys. Res*. *Atmos.*, **104**, 22,301−22,318, https://doi.org/10.1029/1999JD00450.

Zou, X., Wang B., Liu H., Anthes R., Matsumura T., and Zhu Y.-J. (2000) Use of GPS/MET refraction angles in 3D variational analysis. *Q. J. Roy. Meteor. Soc.*, **126**, 1–28, https://doi.org/10.1002/qj.49712657003.

Zou, X., Liu H, Anthes R., Shao H., Chang J.C., and Zhu Y.-J. (2004) Impact of CHAMP radio occultation observation on global analyses and forecasts in the absence of AMSU radiance data. *J. Meteor. Soc. Japan*, **82**, 533–549, https://doi.org/10.2151/jmsj.2004.533.

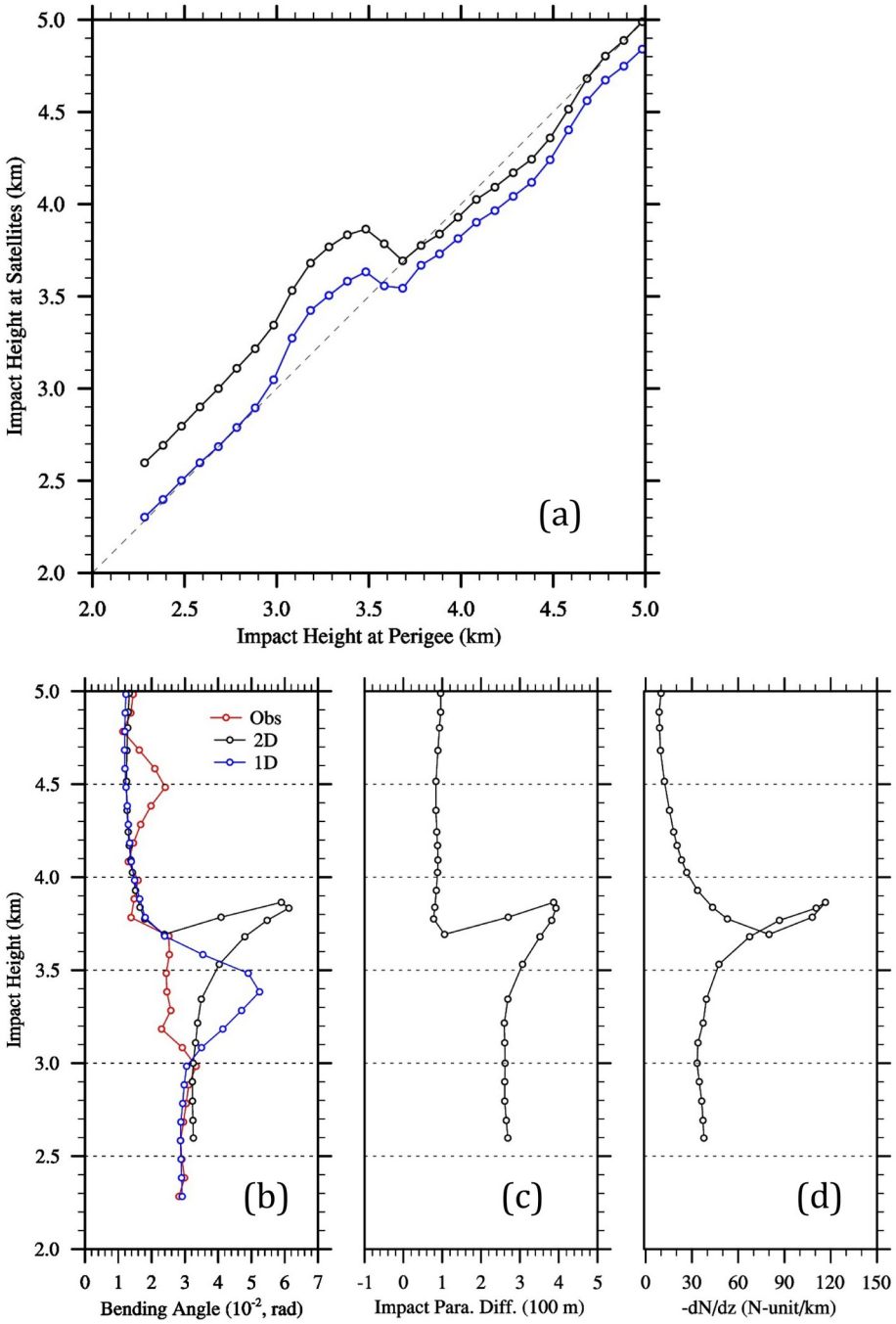

QJ_3520_f1.jpg

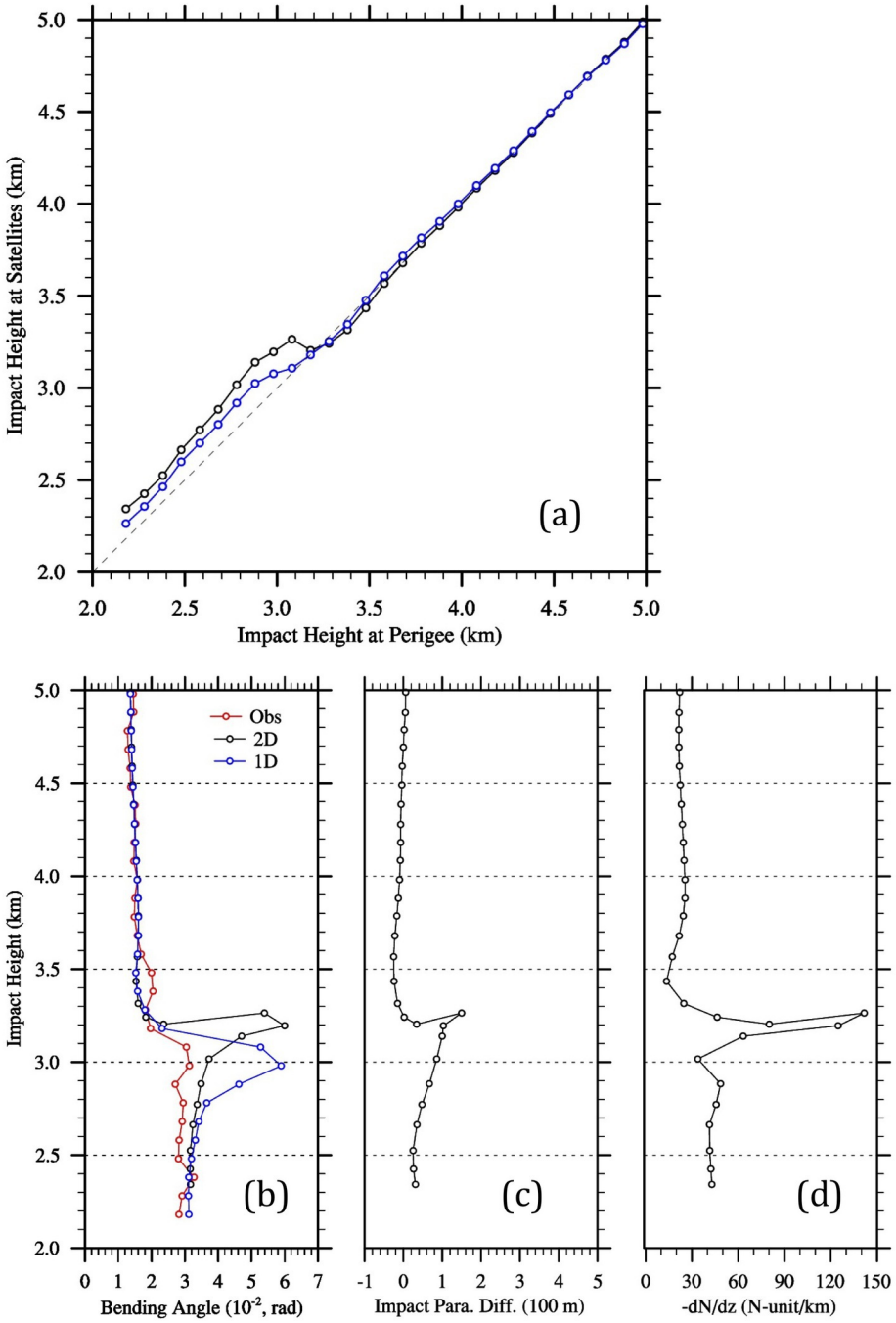

QJ_3520_f2.jpg

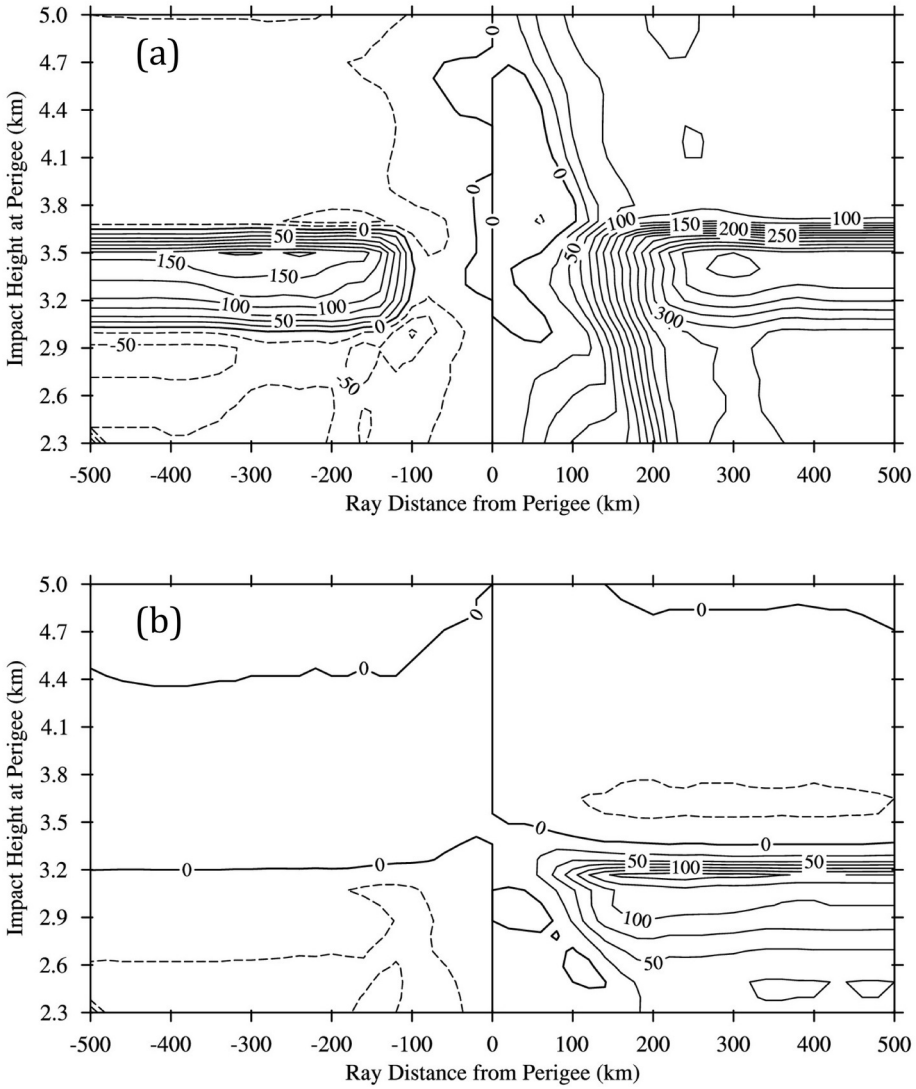

QJ_3520_f3.jpg

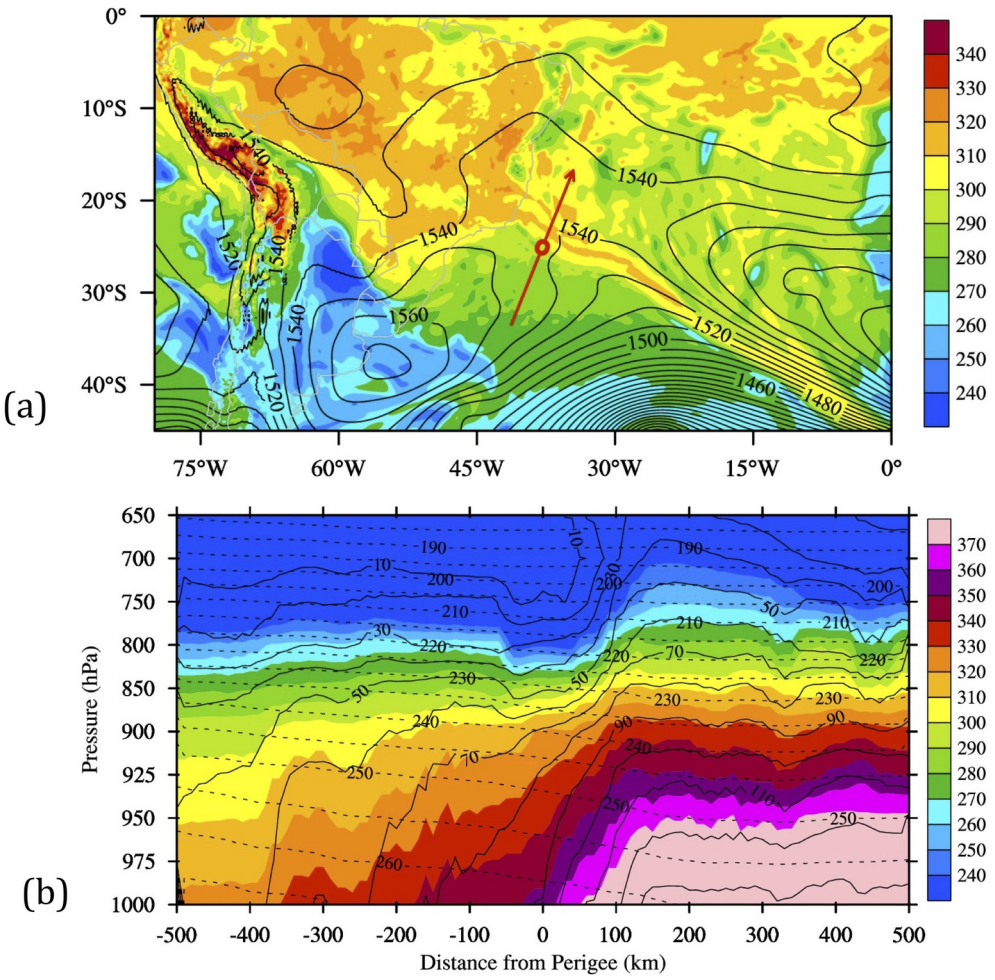

QJ_3520_f4.jpg

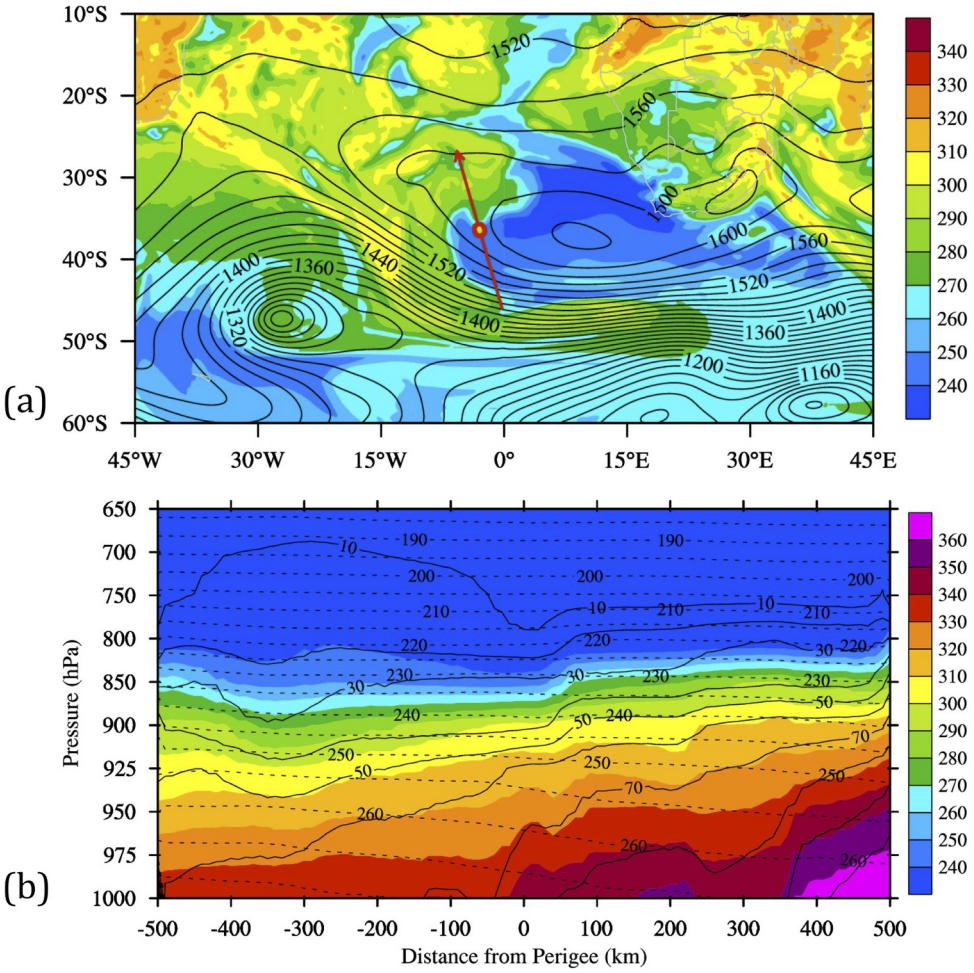

QJ_3520_f5.jpg

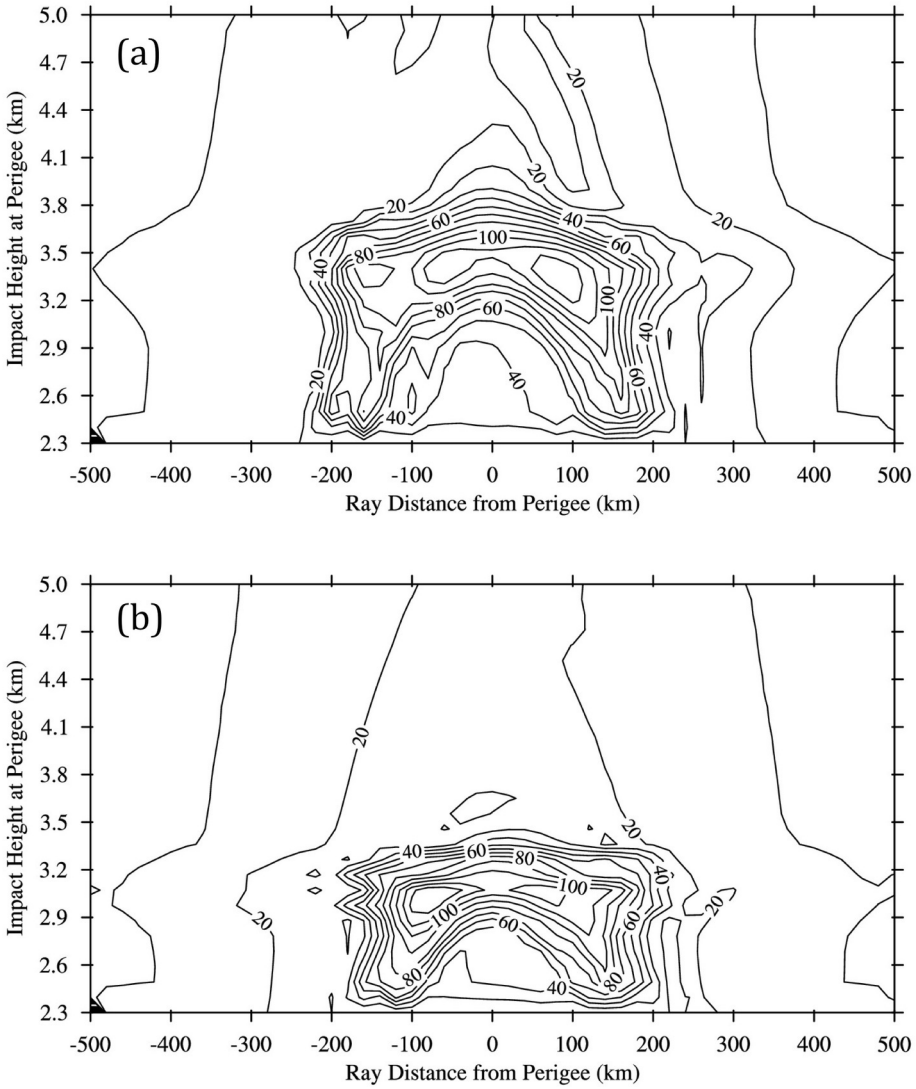

QJ_3520_f6.jpg

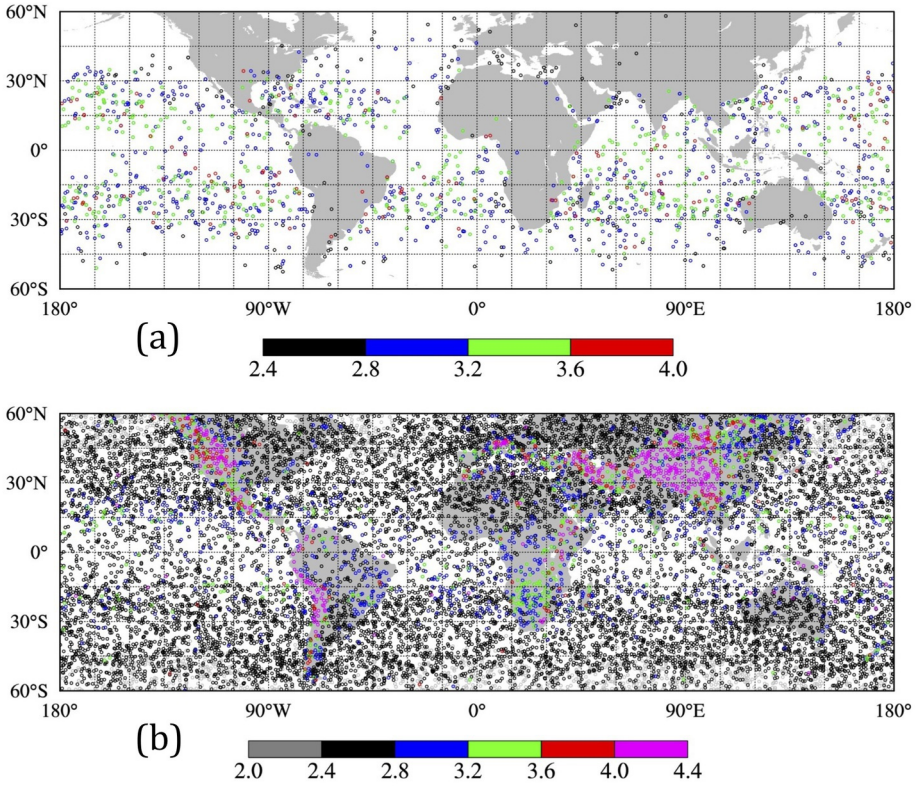

QJ_3520_f7.jpg

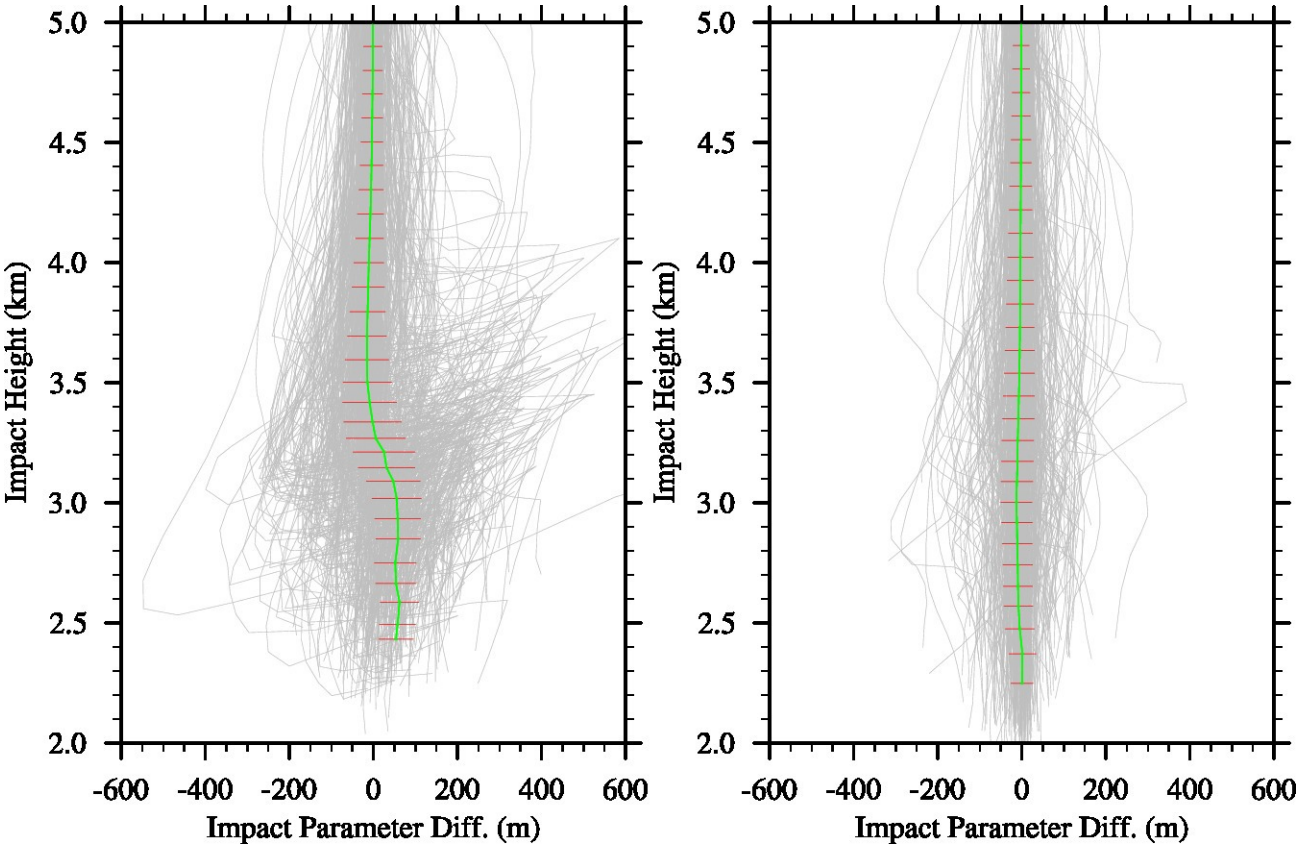

QJ_3520_f8.jpg

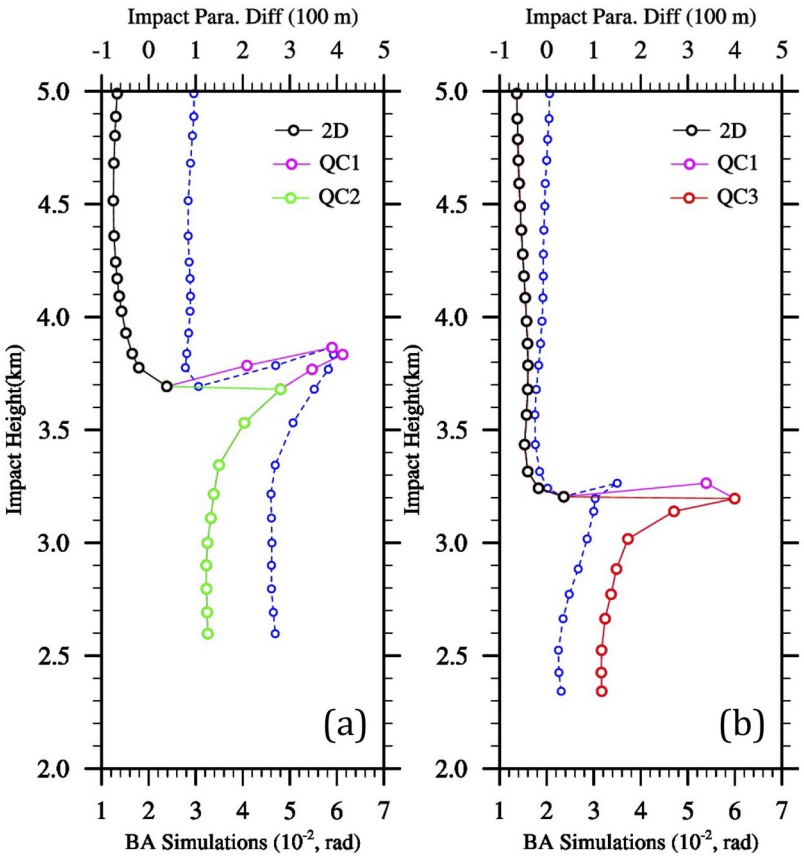

QJ_3520_f11.jpg

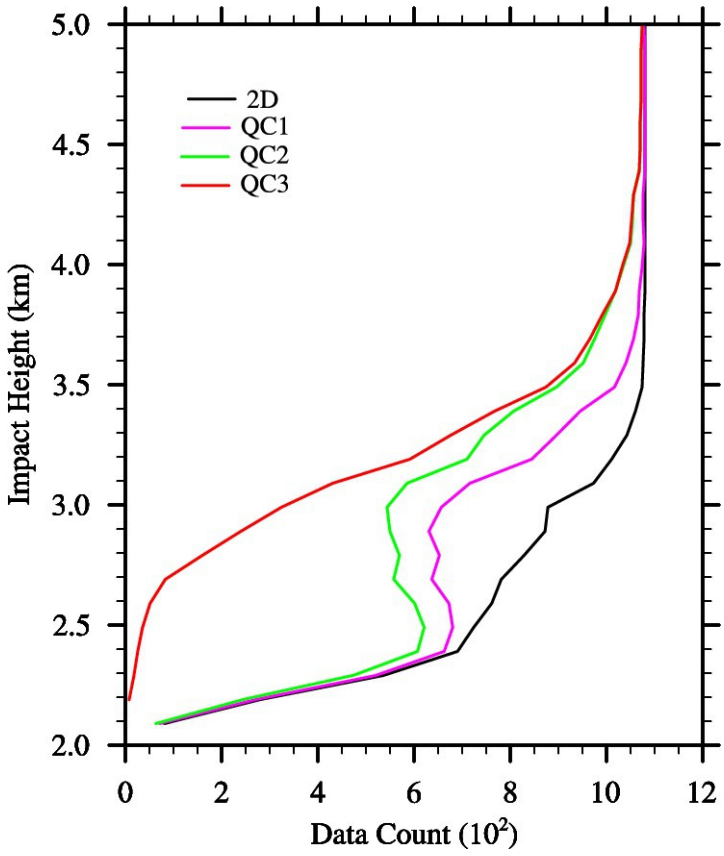

QJ_3520_f13.jpg

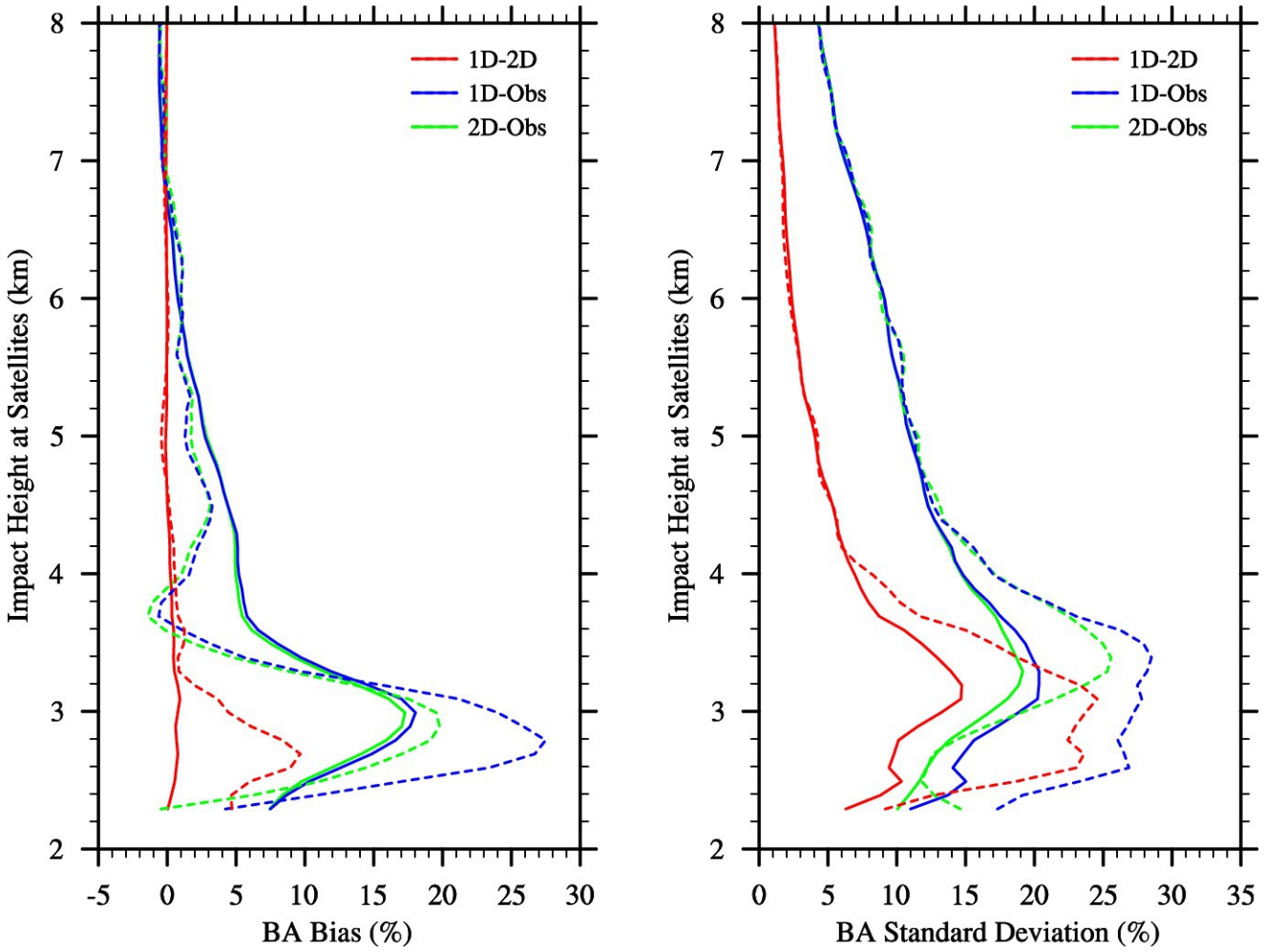

QJ_3520_f14.jpg

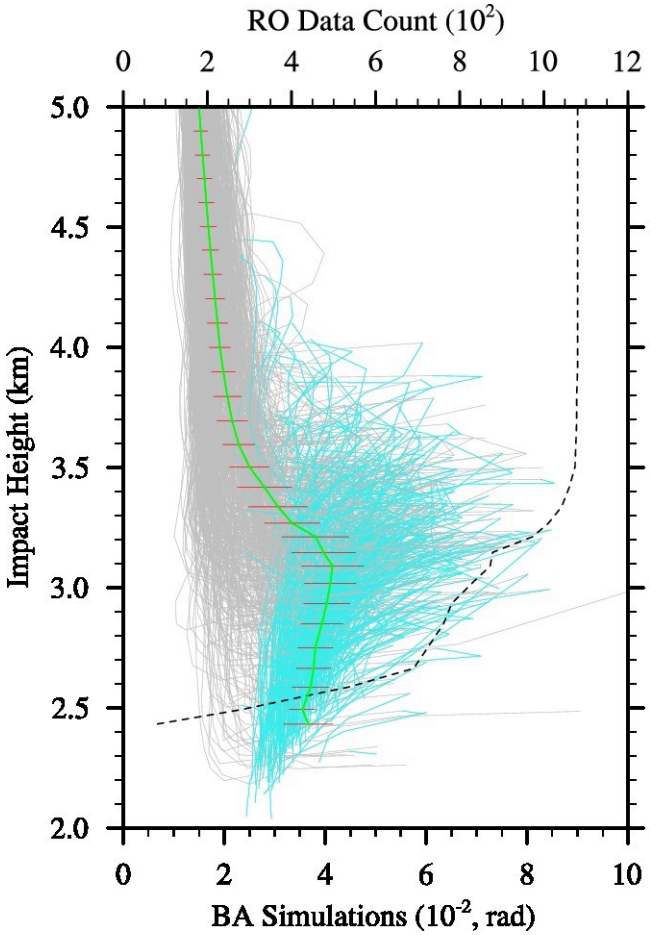

QJ_3520_ZOU_Fig9a.jpg

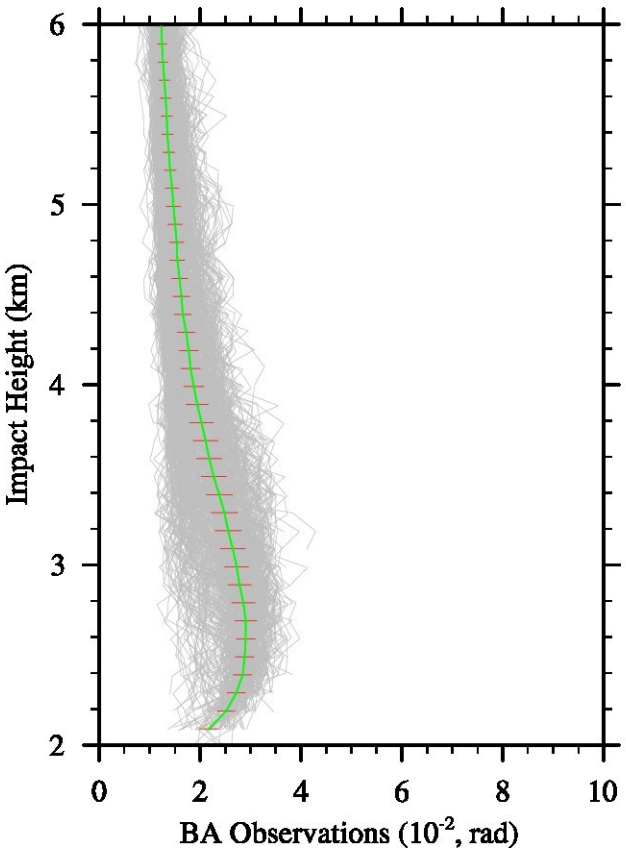

QJ_3520_ZOU_Fig9b.jpg

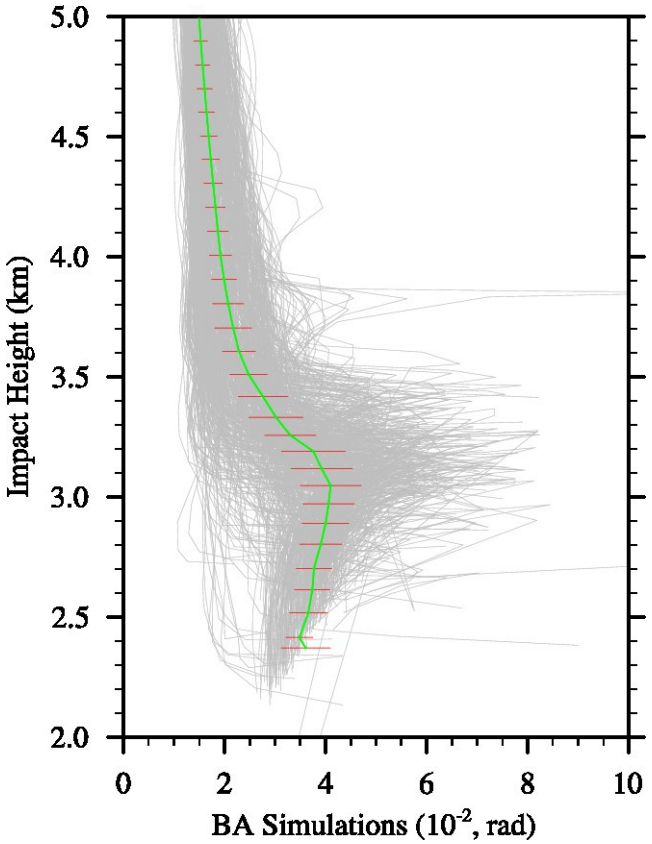

QJ_3520_ZOU_Fig10a.jpg

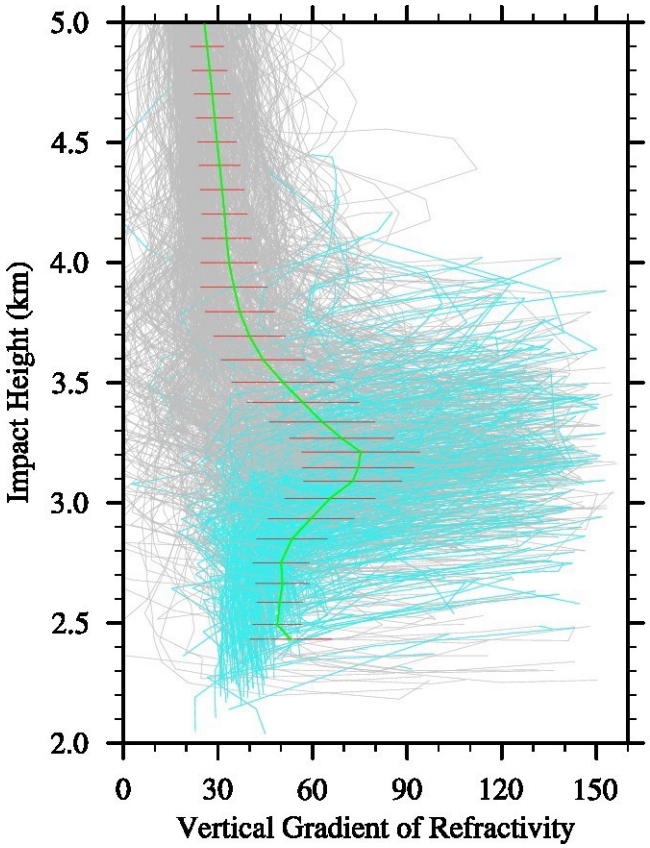

QJ_3520_ZOU_Fig10b.jpg

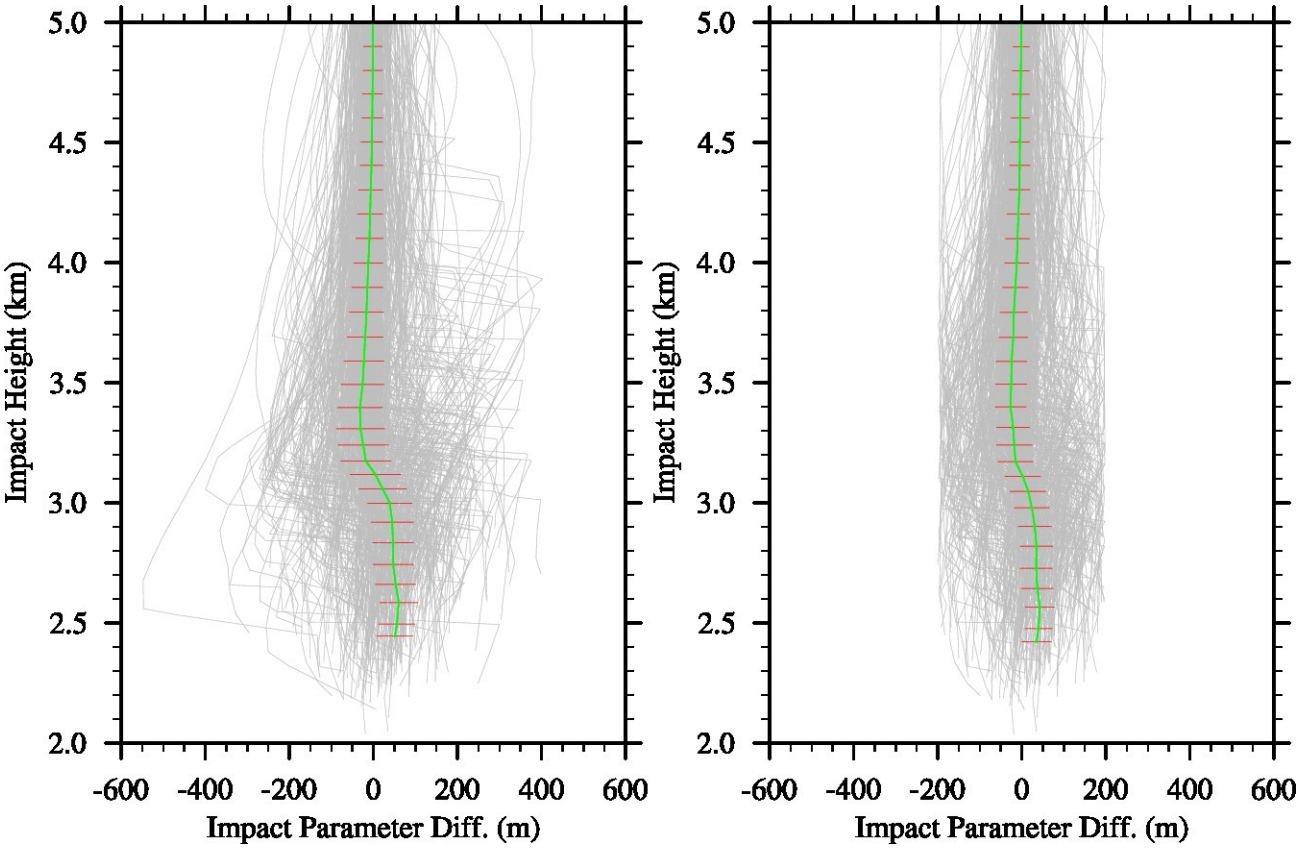

QJ_3520_ZOU_Fig12a.jpg

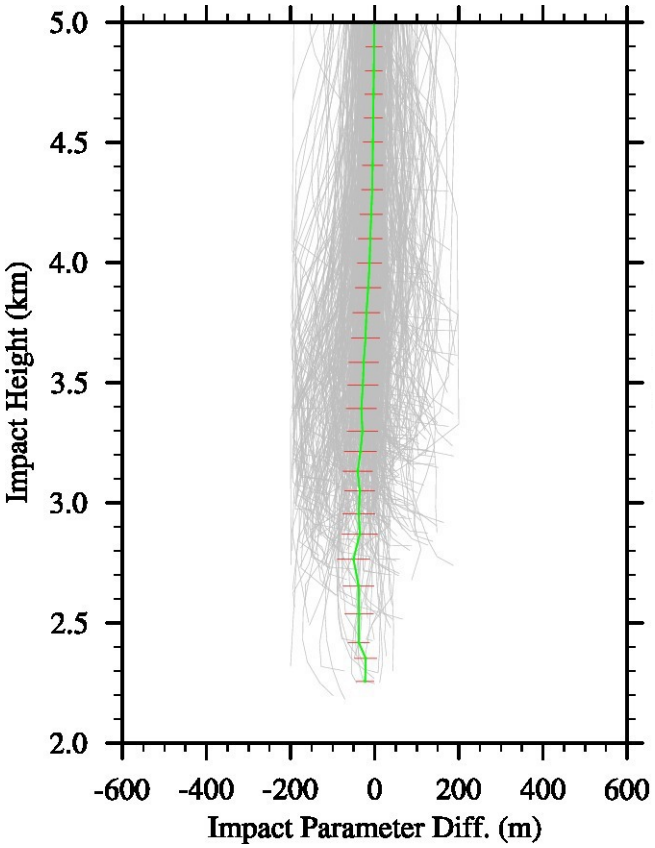

QJ_3520_ZOU_Fig12b.jpg